2. Strength envelope of concrete

To simulate the change of material properties in concrete according to the stress state, accordingly, the biaxial failure envelope should be defined and, in advance, a concrete damage model must be introduced in connection with the biaxial failure envelope. Since the strain rate effect has been controlled by the lateral pressure ratio, in addition to an increase of the uniaxial compressive and tensile failures of concrete with an increasing strain rate, the failure envelope of concrete in biaxial stress states must include both the strain rate and the lateral confining pressure. The equation proposed by Yan and Lin (2007) is modified in this research by excluding the second term related to the strain rate has been given as

$$\frac{f_d}{f_s} = P_1 + P_2 \log\left(\frac{\dot{\varepsilon}}{\dot{\varepsilon}_s}\right) + \frac{P_3}{(1+\alpha)^2} + \frac{P_4\alpha}{(1+\alpha)^2} \tag{1}$$

where f_d and f_s are the dynamic strength of concrete in a biaxial stress state and the uniaxial strength of concrete under quasi-static loading, $\alpha = \sigma_1 / \sigma_2$ $(|\sigma_1| \geq |\sigma_2|)$ is the stress ratio, $\dot{\varepsilon}$ and $\dot{\varepsilon}_s = 10^{-5} s^{-1}$ are the current strain rate and the quasi-static strain rate, and P_1 , P_2, P_3 and P_4 represent parameters associated with material properties. By fitting to the test data, P_1 , P_2, P_3 and P_4 were determined as -0.446, 0.0875, 1.43, and 6.42, respectively, and Eq. (1) shows good agreement with the test data for the change of the strain rate.

However, Eq. (1) not only shows a large difference from Kupfer's failure envelope, which accurately represents the ultimate strength of concrete in a biaxial static stress state when $\dot{\varepsilon} = \dot{\varepsilon}_s$, but also gives a slightly conservative estimation of the dynamic uniaxial strength of concrete [12]. This means that additional modification of Eq. (1) may be required to define the biaxial strength envelope to effectively trace the change in the compressive strength of concrete in a biaxial dynamic stress state. Since Eq. (1) still can effectively simulate the biaxial loading effect, the equation excluding the second term related to the strain rate first has been given as $R(\alpha) = P_1 + \frac{P_3}{(1+\alpha)^2} + \frac{P_4\alpha}{(1+\alpha)^2}$ with the modified values of $P_3 = 1.446$ to satisfy the uniaxial compressive strength condition. The strain rate effect has been taken into account while defining the dynamic uniaxial compressive strength, and the HJC model of $g(\dot{\varepsilon}) = \left(A + BP^{*N}\right)\left(1 + C\ln(\dot{\varepsilon}^*)\right)$ is adopted in this paper upon determining the material constants *A, B, C* and *N* through an experiment (Kwak and Gang 2015) that consists of the SHPB (Split Hopkins Pressure Bar) test for strain rates ranging from 100/s to 800/s, where $g(\dot{\varepsilon}) =$ the dynamic increase factor for the uniaxial compressive strength (see Fig. 1), $P^* =$ normalized pressure for uniaxial stress state, and $\dot{\varepsilon}^* =$ normalized strain rate. Taking the linear product of two independent functions, the modified strength

envelope in the biaxial compressive stress state has been introduced in this paper as $f(\alpha,\dot{\varepsilon}) = g(\dot{\varepsilon}) \cdot R(\alpha)$.

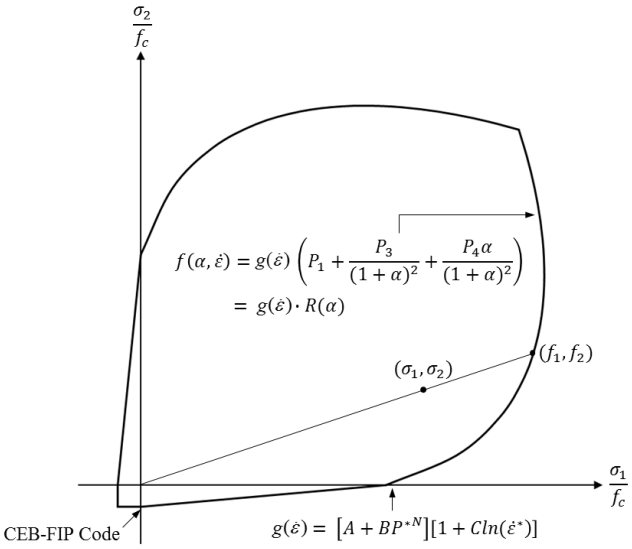

Fig. 1 Biaxial strength envelope of the orthotropic model

Differently from the biaxial compression region, no experiment has been conducted to define the dynamic strength envelope in the compression-tension and biaxial tension regions. However, the dynamic biaxial stress states in the biaxial compression region make it possible to infer the stress states at the other regions. As was adopted in the compression-tension region under the static biaxial stress state (Kwak and Gang 2015), the linear relation that connects the dynamic uniaxial compressive strength and tensile strength has been adopted, upon defining the dynamic tensile strength by the CEB-FIP model code (1993). Under the dynamic biaxial tension, concrete is assumed to exhibit constant dynamic tensile strength compared with that under uniaxial loading. Fig. 1 shows the dynamic biaxial strength envelope constructed in this paper.

Upon defying the biaxial strength envelope for the two principal stress components of σ_1 and σ_2, the other stress component of σ_3 must additionally be considered to represent the complete three-dimensional strength envelope. To take into account the triaxial stress effect, accordingly, another function, $h(\sigma_3 / f_c)$, which has been expressed in terms of the other stress σ_3, has been designed in this paper on the basis of the triaxial experimental data (Mills and Zimmerman 1970). The circular dots in Fig. 2, which show the experimental data, represent an increase of the biaxial compressive strength to the biaxial strength envelope defined with $R(\alpha)$. That is, the dot denotes the ratio of $\overline{OB}$ to $\overline{OA}$ in Fig. 3 when $g(\dot{\varepsilon}) = g(0)$, representing the static stress condition. The variation of the biaxial strength envelope has been drawn with respect to the normalized third stress component of σ_3 / f_c, as shown in Fig. 2, and

then the linear regression of the ratio gives the expression of another function, $h(\sigma_3 / f_c)$ in Fig. 2. On the other hand, because all the experiments were performed in the triaxial compression state of stress, the failure criterion proposed by Ottosen (1975) (whereas the experimental data used here were also based on the development of the K&C model) has been used as a reference to compare the relative magnitude of the decreasing rate for the triaxial strength envelope of concrete between the proposed function of $h(\sigma_3 / f_c)$ and Ottosen's criterion, when the third stress σ_3 is the tensile stress. Ottosen's failure criterion defined as a four parameter criterion satisfies all the required properties in the yielding surface such as smoothness, convexity, symmetry and curved meridians and gives a good agreement with experimental failure stresses under general stress states. However, because the triaxial loading effect is different from that in the compressive stress range of σ_3, a different regression equation of $h(\sigma_3 / f_c)$ has been defined in the tensile stress range of σ_3. Accordingly, the multiplication of $h(\sigma_3 / f_c)$ by the equation for the biaxial strength envelope $f(\alpha)$ finally represents the triaxial strength envelope of concrete in the triaxial compression region (see $s(\alpha, \dot{\varepsilon}, \sigma_3 / f_c) = h(\sigma_3 / f_c) \cdot f(\alpha, \dot{\varepsilon})$ in Fig. 3).

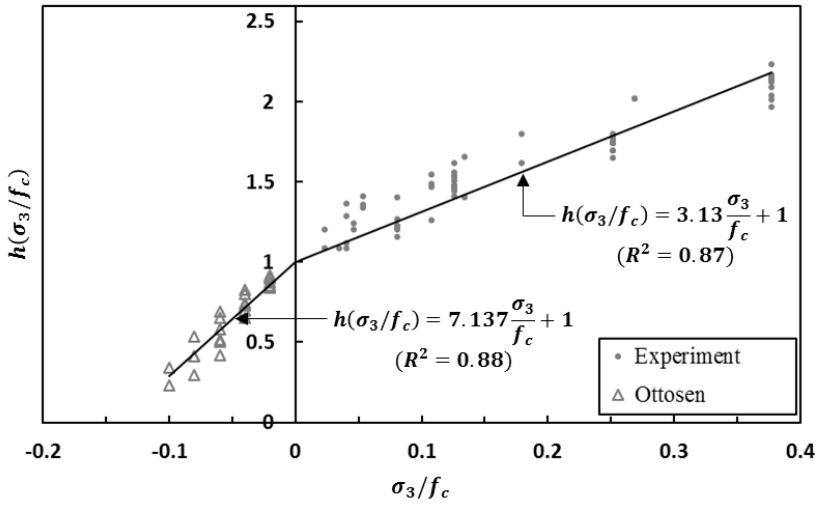

Fig. 2 Regression relation for $h(\sigma_3 / f_c)$

However, a similar increase or decrease of the strength envelope cannot be expected for the triaxial tension state of stress, analogous to the biaxial tension state of stress. Accordingly, no change of the strength envelope has been assumed in the triaxial tension region regardless of the magnitude of the third tensile stress. Since the linear relation was adopted in the compress ion-tension region under the biaxial stress state (see Fig. 1), this linear relation in defining the compression-tension state of stress has been assumed to be maintained in the triaxial stress state. Fig. 3 shows the finally constructed triaxial strength envelope.

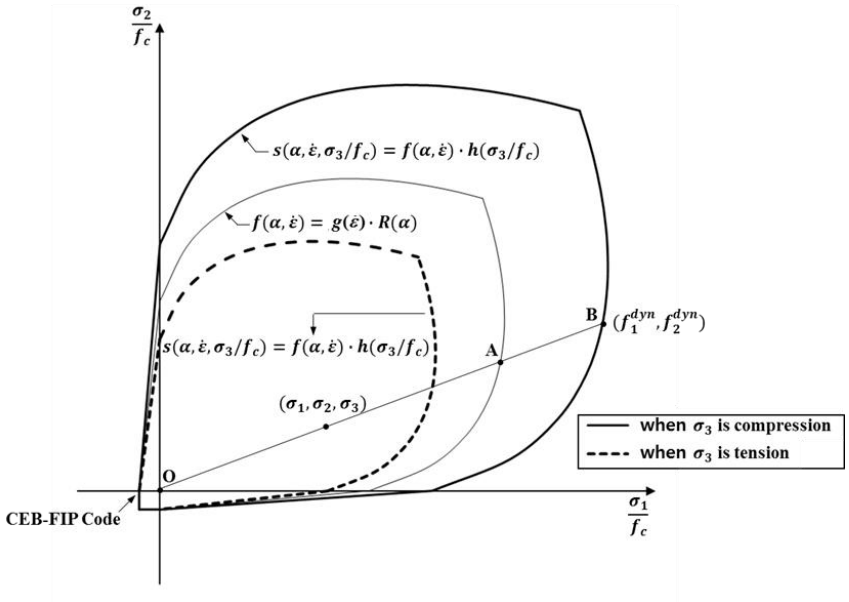

Fig. 3 Triaxial strength envelope of the orthotropic model

3. Numerical analysis

In order to verify the accuracy of the proposed orthotropic model in predicting structural behavior under impact loading, numerical analyses have been performed for a RC slab tested by Hanchak et al. (1992) using LS-DYNA 971 along with a comparison of the numerical results to the concrete damage models of HJC (Type 111 in LS-DYNA), CSC (Type 159 in LS-DYNA), and K&C (Type 72 in LS-DYNA), which are widely adopted to trace the cracking behavior of concrete structures subjected to impact loading, has been performed. Moreover, the sensitivity of the FE mesh size in relation to the numerical results is examined by using three different sizes of solid elements in numerical simulations. This numerical simulation for a RC slab has been used by other researchers [44, 45] as benchmark experimental results to verify their numerical models. The slab is composed of concrete with uniaxial compressive strength of 48MPa and has dimensions of 610 X 610 X 178 mm. In the experiments, the slab is subjected to impact loading delivered from 0.5 kg ogival-nose steel projectiles. In advance, the proposed orthotropic model is implemented as a user-defined concrete material model in LS-DYNA, and the evaluation of the stresses follows the steps mentioned in the “solution procedure” in this paper. In advance, the Von-Mises criterion is used to trace the material behavior of the steel projectile.

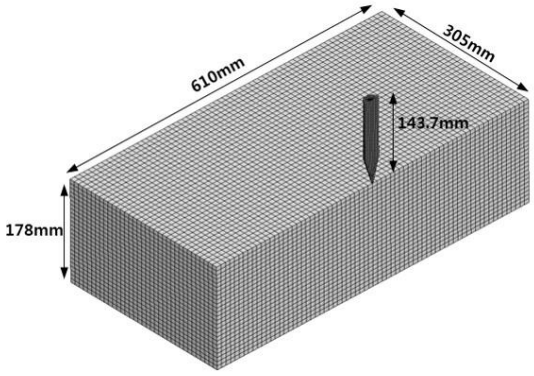

Fig. 4 Finite element idealization of projectile and target

The finite element model in Fig. 4 represents only half of the target structure and the projectile, taking advantage of the symmetry in geometry and loading, and it has been constructed by using the pre-processor Hyper-Mesh. The reinforcing steel placed in concrete is also considered in the FE analyses on the basis of the one-dimensional truss model constrained in solid elements.Three dimensional constant stress solid elements (SOLID 1 in LS-DYNA) are used in the finite element discretization, and three different sizes of solid elements with dimensions of 6 mm height and 6.1 mm width and length (Mesh A), 8.7 mm width and length (Mesh B), and 12.2 mm width and length (Mesh C) are used for the concrete target to examine the numerical error according to the FE mesh size. It should be noted that the analyses have been performed by changing the size of a finite element in the width and depth directions because the numerical error will be more sensitive to the variation of the FE mesh size in these directions rather than that in the height direction, as was discussed in a previous study (Kwak and Gang 2015). Since the experiment was conducted with variation of the striking velocities ranging from 300 m/s to 1000 m/s and then the corresponding residual velocities were measured, a comparison of the numerical results to the experimental data has been made for the residual velocities of the projectile after perforation of the concrete target because the residual velocity of the projectile maintains a constant value. Figs. 5 (a) to (c) show the numerical predictions of the residual velocity compared with the experimental data and the predictions obtained by the conventional plasticity based concrete damage models with respect to the FE mesh size used in the numerical analysis. The application of the plasticity based damage models of HJC, K&C, and CSC is based on the use of a fixed value, $\varepsilon_{cu} = 0.01$ for the failure strain regardless of the FE mesh size, according to the recommendation proposed for each plasticity based model (Holmquist et al. 1993, Schwer and Malvar 2005, Murray 2007). As shown in these figures, the proposed orthotropic concrete model (continuous lines in Figs. 5 (a) to (c)) not only gives very satisfactory agreement between the results of the analyses and the experiment data through the entire velocity range but also shows less sensitivity to the variation of the FE mesh size used in the numerical analyses. On the other hand, the plasticity based damage models still give an accurate prediction of the experimental data at the relatively small FE mesh size, but this accuracy decreased with an increase of the FE mesh size.

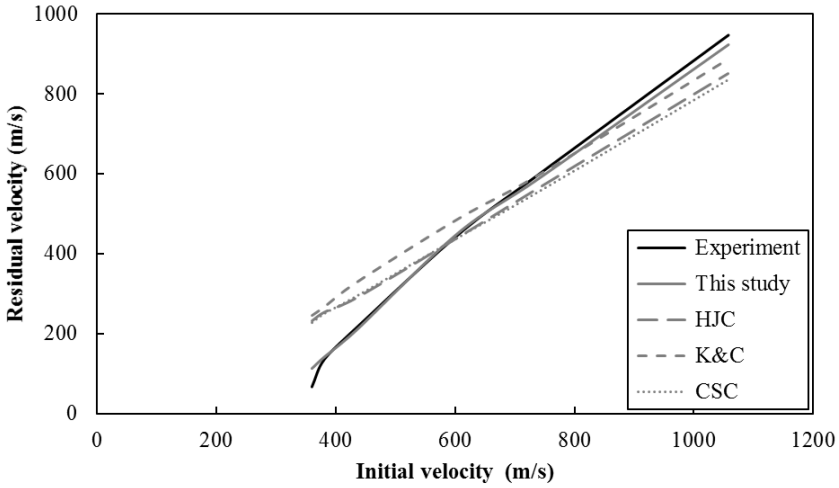

(a) Usig Mesh A

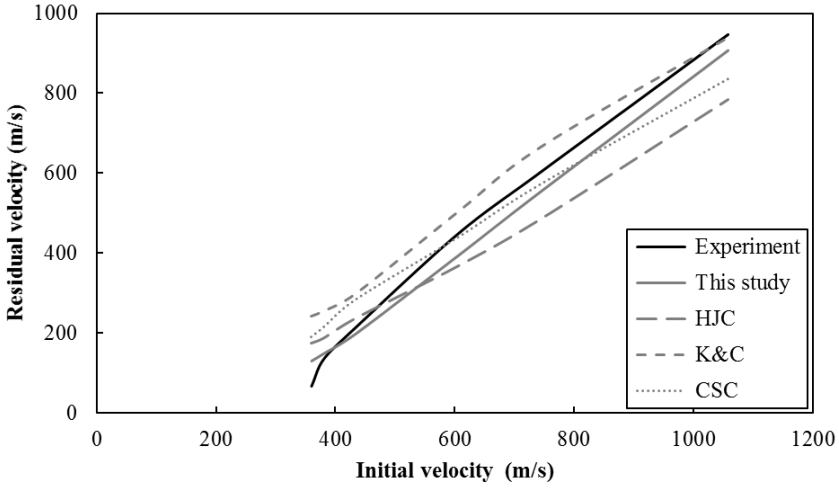

(b) Usig Mesh B

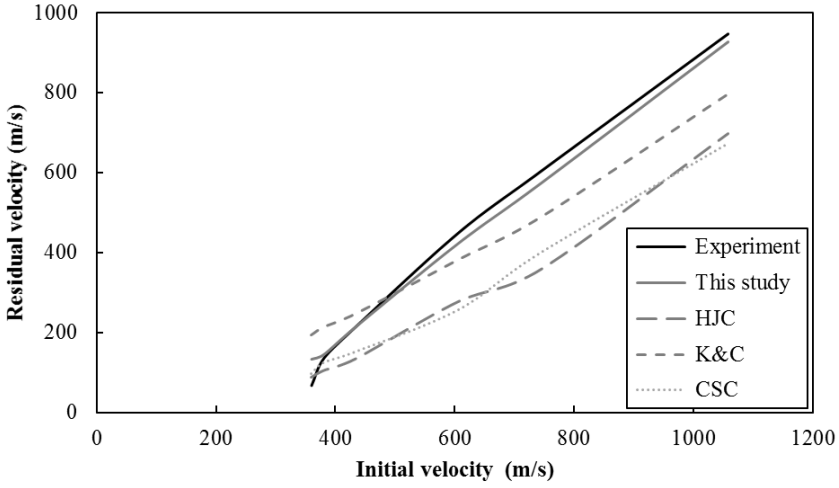

(c) Using Mesh C

Fig. 5 Comparison of residual velocity to initial velocity

5. CONCLUSIONS

This paper introduces an orthotropic concrete material model to describe the nonlinear behavior of concrete structures subjected to impact loading. The efficiency of the proposed model in reducing the mesh dependency and its accuracy in the prediction of concrete structural behavior under impact loading are verified by comparing the analytical prediction with experimental results obtained from the perforation test of a concrete slab subjected to a projectile impact. The results show that the proposed model reasonably reflects the multi-axial dynamic behavior of concrete and the accuracy of the simulation results is dramatically improved regardless of the FE mesh size used in the numerical analyses.

ACKNOWLEDGMENT

This research was supported by a Construction Technology Research Project (17SCIP-B128706-01) funded by the Ministry of Land, Infrastructure and Transport.

REFERENCES

Bischoff P.H. and Perry SH. (1991), “Compressive behavior of concrete at high strain rates”, *Material and structure,* **24**(6), 425-450.

Yan D. and Lin G. (2007), “Dynamic behavior of concrete in biaxial compression”, *Magazine of Concrete Research,* **59**(1), 42-52.

Mills L.L., Zimmerman R.M. (1970), “*Compressive strength of plain concrete under multiaxial loading conditions”, ACI J*, **67**(10),802-807.

Kwak H.G. and Gang H.G. (2015), “A bi-axial model for concrete under high-strain rate conditions” Materials characterisation 2015. Wessex institute of technology, 319-330.

Kwak H.G. and Gang H.G. (2015), “*An improved criterion to minimize FE mesh-dependency in concrete structures under high strain rate conditions”, International Journal of Impact Engineering*, Vol. **86**, 84-95.

CEB-FIP (1993), “*CEB-FIP Model Code 1990*”, *Design Code,* **25**(1).

Ottosen N.S. (1975), “Failure and Elasticity of Concrete”, Danish Atomic Energy Commission, Research Establishment Risö, Risö-M-1801, September 1975;67.

Hanchak S.J. et al. (1992), “*Perforation of concrete slabs with 48 MPa (7 ksi) and 140 MPa (20 ksi) unconfined compressive strengths”, International Journal of Impact Engineering*, **12(1)**, 1-7.

Holmquist T.J., Johnson G.R., Cook W.H. (1993), “A computational constitutive model for concrete subjected to large strains, high strain rates, and high pressure”, international symposium on ballistics. Quebec, Canada. International Ballistics Society, 591-600.

Schwer L.E. and Malvar, L.J. (2005), “*Simplified concrete modeling with* MAT_CONCRETE_DAMAGE_REL3*”, *JRI LS-Dyna User Week.*

Murray Y.D. (2007), “*Users manual for LS-DYNA concrete material model 159. Rep. No. FHWA-HRT-05-062*”, *Federal Highway Administration,* 1-77.